ELKHA : Jurnal Teknik Elektro, Vol. 15 No.1, April 2023, pp. 11 - 17
ISSN: 1858-1463 (print), 2580-6807 (online)

Analysis of ITO/a-Si:H(p)/a-Si:H(i)/c-Si(n)/Al HIT (Heterostructure with Intrinsic Thin Layer) Solar Cell Performances

Igor Levi Satriani[1)], Rahmawati Munir[2)], Adrianus Inu Natalisanto[3)], and Dadan Hamdani[4*)]

[1,2,3,4)] Theoretical and Material Physics Laboratory, Department of Physics, Mulawarman University, Indonesia
Corresponding e-mail: [*)] dadanhamdani@fmipa.unmul.ac.id

***Abstract* – Numerical simulation on Heterostructure with Intrinsic Thin Layer (HIT) solar cell using hetero-structure ITO/(p^+)a-Si:H/(i)a-Si:H/(n)c-Si/Al solar cell has been done using Automate For Simulation of Heterostructure (AFORS-HET) software. The purpose of this study is to provide validation as well optimization model of solar cell enhanced performances. Data analysis shows a significant increase on solar power generation. An intrinsic thin layer given between the hetero-interface to reduce defect properties on solar cell structure. The optimization using an optimal value of acceptor-donor doping, dangling-bond defects (N_{tr}), thin conductive oxide work function (WF_{TCO}), and other input shows a reducing recombination-rates, as a validation Figure of Merits (FOMs) data reach a maximum efficiency value at 23.67% (V_{OC} = 634.2 mV; J_{SC} = 51.2 mA/cm^2; FF = 72.91%, this result achieve peak data as follows WF_{TCO} = 5.2 eV, Na (doping) = 5.0 x 10^{19} cm^{-3}, WF_{TCO} = 1.0 x 10^{18} cm^{-3}, D_{it} (interface defect) = 1.0 x 10^{10} cm^{-3}. The results obtained from this simulation produce a number of optimum parameters that can be followed up experimentally to obtain better solar cell performances.**

Keywords: AFORS-HET, efficiency, heterostructure, solar cell.

I. INTRODUCTION

Photovoltaic was an alternative solution to cope with the increasing energy consumption. To this day various kind of photovoltaic technology have been invented. Thin film solar cell for instance, had a potential to compete the current commercial solar cell due to higher performance of efficiency [1]. However, there is a problem within wide usage of thin film technology, highly market value caused by overprice material could be a troublesome to use publicly. Crystalline silicon (c-Si) solar cell technology for example, has a large expense for installment and material fabrication. On the other hand using material such as hydrogenated amorphous silicon with lower cost fabrication, fabricated on much lower temperature, wide energy gap (between 1.7 eV to 2 eV) and greater light absorption could be more suitable for reducing solar cell pricing problem [2]. The drawback factor using this material was the low efficiency percentage compared to other solar cell materials, this was caused by light-induced degradation during illumination process on panel. Single-junction p-i-n solar cell of a-Si:H had a highest efficiency record by 10.3% [3].

In addition, the quality of (i)a-Si:H layer plays an important role in obtaining high efficiency solar cells. Besides have good electrical transport properties to enable photo-generated electrons and holes to exit the device before recombination, it also has good light absorption properties to produce as many electron-hole pairs as possible at a given light intensity with phosphorus doping of the (i)a-Si:H layer about 2.0 x 10^{18} atom/cm^3 with a conversion efficiency of 8.85% (V_{OC} = 0.68 V, J_{SC} = 19.43 mA/cm^2, FF = 0.67) [4]. Reported that by the addition of an intrinsic layer (with a different bandgap) to the a-Si:H p-i-n solar cell structure was deposited using rf-PECVD techniques, the conversion efficiency of the new structure (p-i_1-i_2-n solar cell) is enhanced from 5.61% to 8.86% [5]. The conversion efficiency of a-Si:H solar cells is still low compared to crystalline-based solar cells. So, it is necessary to increase it by combining the two materials to produce a silicon-heterojunction (SHJ) solar cell that is capable of producing a conversion efficiency of 26.3% with excellent passivation of c-Si by thin film a-Si:H contacts for electrons and holes with Heterojunction-interdigitated back contact (HJ-IBC) technology [6]. Reported influences of TCO/(a)-Si:H low contact resistivity can be achieved by net doping of (p)a-Si:H layer which dopant concentration was about 1.9 x 10^{20} cm^{-3} which is reduced by defect creation [7].

In this study, by using numerical simulation the HIT performances were investigated by using AFORS-HET software. Various input parameters added on the simulation, resulting data analysis such as band-energy diagram, recombination rate, electrical field profile, short circuit current, even carrier concentration to visualize the influence of input parameter variant on solar cell.

II. METHODOLOGY

A. *Methodology*

Automate FOR Simulation of Heterostructure (AFORS-HET) is used to simulate and optimize solar cell capability. Using different analysis, the results will be a reference for experimental fabrication. Structure of this solar cell consist of a-Si:H on both **p**$^+$ (10nm) and **i** (5nm) layers. For hetero junction, a silicon crystalline c-Si (200 μm) was used. An intrinsic thin layer with 3 nm thickness

Manuscript received 2023-01-14; revised 2023-03-06; accepted 2023-03-14

placed within the hetero interface described in Figure 1. Using a suitable ideal illumination, simulation has been done with a stable temperature at about 300 K and Air Mass Coefficient set to 1.5 AM [8]. Table 1 shows the typical parameters used in the simulations in more detail, as described in previous studies [9], [10].

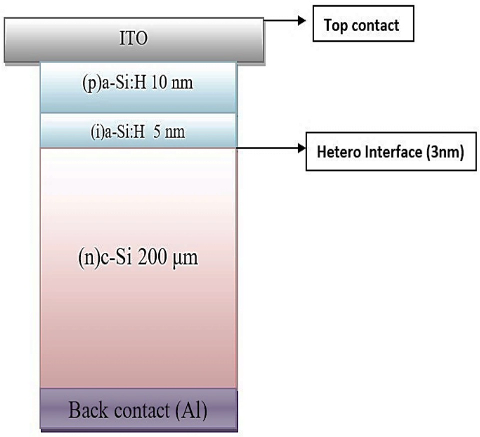

Figure 1. Visualization of HIT solar cell structure used

Simulation model using analysis of Figure of Merits (FOMs) was carried out to observe solar cell performance optimization. This will explain some electrical changes over the simulation process by various input parameters, resulting in an electrical difference on V_{OC}, J_{SC}, *FF* and *Eff*, as shown in equations (1-4). Those data used to represent value of solar cell energy conversion efficiency depicted on J-V curve diagram [11].

$$J_{sc} = J_{ph} - J_0\,(e^{\frac{qV_{oc}}{nKT}} - 1) \quad (1)$$

$$V_{oc} = \frac{nkT}{qV_{oc}} \ln\left(\frac{J_{ph}}{J_0} + 1\right) \approx \frac{nkT}{qV_{oc}} \ln\left(\frac{J_{ph}}{J_0}\right) \quad (2)$$

$$FF = \frac{P_m}{J_{sc}x\,V_{oc}} = \frac{J_m x V_m}{J_{sc} x V_{oc}} \quad (3)$$

$$Eff = \frac{V_{mpp} I_{mpp}}{P_{illumination}} = \frac{FF\,V_{oc} I_{sc}}{P_{illumination}} \quad (4)$$

Equation (5) is electrical model used on each layer based on continuity and Poisson equation to describe electron and hole state, Poisson equation used in simulation is as follows [12] .

$$\frac{\varepsilon_o \varepsilon_r}{q} \frac{\partial^2 \phi(x,t)}{\partial x^2} = p(x,t) - n(x,t) + N_D(x) - N_A(x) + \sum_{trap} \rho_{trap}(x,t) \quad (5)$$

where q as electric carrier, $\varepsilon_o \varepsilon_r$ as absolute and relative dielectric, defect density on carrier defect $\rho_{trap}(x,t)$ depends on defect type also the value of local carrier density $n(x,t)$; $p(x,t)$. Continuity equation for electron and hole within 1D dimension written on these equations (6-7) [10], [12].

$$-\frac{1}{q}\frac{\partial j_n(x,t)}{\partial x} = G_n(x,t) - R_n(x,t) - \frac{\partial}{\partial t} n(x,t) \quad (6)$$

$$+\frac{1}{q}\frac{\partial j_p(x,t)}{\partial x} = G_p(x,t) - R_p(x,t) - \frac{\partial}{\partial t} p(x,t) \quad (7)$$

where Generation rate value $G_n(x,t)$; $G_p(x,t)$ is obtained by calculating optical model, while $R_n(x,t)$ and $R_p(x,t)$ are recombination rate. Electron-hole current $j_n(x,t)$; $j_p(x,t)$ owned with gradient of fermi energy $E_{Fn}(x,t)$; $E_{Fp}(x,t)$.

Fermi-Dirac distribution function approach has been done with using Maxwell-Boltzmann equation to obtain dependent fermi energy position also value of the local electron-hole current as described equations (8-11) [11]–[13].

$$E_{Fn}(x,t) = E_C(x) + kT \ln\frac{n(x,t)}{N_C(x)} = -\,q\chi(x) + q\varphi(x,t) + kT\,\ln\frac{n(x,t)}{N_V(x)} \quad (8)$$

$$E_{Fp}(x,t) = E_V(x) + kT \ln\frac{p(x,t)}{N_V(x)} = -\,q\chi(x) + q\varphi(x,t) - E_g(x) + +kT\,\ln\frac{P(x,t)}{N_V(x)} \quad (9)$$

$$j_n(x,t) = q\,\mu_n\,n(x,t)\frac{\partial E_{Fn}(x,t)}{\partial x} \quad (10)$$

$$j_p(x,t) = q\,\mu_p\,p(x,t)\frac{\partial E_{Fp}(x,t)}{\partial x} \quad (11)$$

where μ_n,μ_p as electron-hole mobility, χ as electron affinity, E_g; E_C; and E_V are energy gap, conductive band energy, valence band energy, respectively. Effective density of state (DOS) from both valence and conductive band energy are symbolized as $N_c; N_v$. Total recombination rate $R_{n,p}(x,t)$ on semiconductor layer more specifically at photoactive area gained from some of recombination that occurs is described in Equations (12) [13], [14].

$$R_{n,p}(x,t) = R_{n,p}^{BB}(x,t) + R_{n,p}^{A}(x,t) + R_{n,p}^{DB}(x,t) + R_{n,p}^{SRH}(x,t) \quad (12)$$

where the radiative recombination between band energy $R_{n,p}^{BB}(x,t)$; auger recombination $R_{n,p}^{A}(x,t)$; Shockley-read-hall recombination $R_{n,p}^{SRH}(x,t)$; also dangling-bond $R_{n,p}^{DB}(x,t)$, make significant change on solar panels performance.

III. Results and Discussion

Figure 2 shows a different result on solar cell performances by numerous doping N_A. Simulation was done with WF_{TCO} settings on energy level stretched to flat-band so there is no interference within front contact. Doping ranged from lower concentrate 5.0 x 10^{17} until the highest doping 1.0 x 10^{20} cm^{-3} were used in simulation [15]. With AFORS-HET as simulation software, well performed doping which made a significant change obtained at 5x10^{18} cm^{-3} attaining an output V_{OC} = 625.4 mV; J_{SC} = 51.8 mA/cm^2; FF = 48.55% in addition to efficiency of about 15.73%.

The peak solar cell output gained from optimizing the dopant layer had been embodied at N_A = 5.0 x 10^{19} cm^{-3}. Also given doping improved parameters particularly on fill factor, reaching about 74.61 % caused a substantial boost on overall efficiency for 23.88 %. Both different doping concentrations (moderate and high) accustomed for comparison for further simulation. Using optimum doping N_A such as 5 x 10^{18} cm^{-3} and highest output produce on higher doping 5 x 10^{19} cm^{-3}, an analysis was settled to find an ideal well performed WF_{TCO} value for magnifying solar cell output. WF_{TCO} value that used in this simulation varied from 4.7 eV to 5.6 eV. The output presented in Figure 3 shows a significant hike for all parameters on both doping variations. Adding up WF_{TCO} value from the lowest 4.7 eV caused rapid increase on V_{OC} and J_{SC}, mainly affected by a swift transition on Schottky contact to more Ohmic-alike contact in energy level.

The declining trends from Figure 4 explain how different WF_{TCO} values have big impact on peak level performance for solar cell panel output. We could see a wide diverse voltage V_{OC} output causes a significant drop on solar cell work, although slightly diverse on J_{SC} current value output. Using high WF_{TCO} rate (> 5.0 eV) could influence an reverse barrier to ensue, reverse barrier results in a large hole concentrate injected from front contact to semiconductor (p^+)a-Si:H layer.

Table 1. Various parameters input for reconstructing HIT solar cell using AFORS-HET

Parameter	(p^+)a-Si:H	(i)a-Si:H	a-Si:H/c-Si interface	(n)c-Si
Thickness (nm)	10	5	3	2 x 10^5
Dielectric constant	11.9	11.9	-	11.9
Electron affinity (eV)	3.9	3.9	-	4.05
Band gap (eV)	1.72	1.72	-	1.124
Effective cond. band density (cm^{-3})	2.5 x 10^{20}	2.5 x 10^{20}	-	2.846 x 10^{19}
Effective val. band density (cm^{-3})	2.5 x 10^{20} 1.0 x 10^{17}	2.5 x 10^{20}	-	2.685 x 10^{19}
Acceptor concentration, Na (cm^{-3})	5.0 x 10^{17} 1.0 x 10^{20}	0	-	0
Donnor concentration, Nd (cm^{-3})	0	0	-	1.5 x 10^{16}
Electron mobility ($cm^2V^{-1}s^{-1}$)	20	20	-	1111
Hole mobility ($cm^2V^{-1}s^{-1}$)	5	5	-	421.6
Electron thermal velocity (cms^{-1})	1.0 x 10^7	1.0 x 10^7	-	1.0 x 10^7
Hole thermal velocity (cms^{-1})	1.0 x 10^7	1.0 x 10^7	-	1.0 x 10^7
Defect density at the edge of conduction (valence) band ($cm^{-3}eV^{-1}$)	4.0 x 10^{21} (4.0 x 10^{21})	2.0 x 10^{21} (2.0 x 10^{21})	-	1.0 x 10^{14} (1.0 x 10^{14})
Urbach Energy for conduction (valence) tail (eV)	0.06(0.03)	0.094(0.068)	-	-
Capture cross section σ_c (σ) at the edge of conduction band (cm^2)	1.0 x 10^{-17} (1.0 x 10^{-15})	7.0 x 10^{-16} (7.0 x 10^{-16})	-	-
Capture cross section σ_c (σ) for valence band tail (cm^2)	1.0 x 10^{-15} (1.0 x 10^{-17})	7.0 x 10^{-16} (7.0 x 10^{-16})	-	-
Gaussian density of states (cm^{-3})	1.0 x 10^{18} (1.5 x 10^{19})	7.0 x 10^{19}	-	-
Gaussian Energy for donor (acceptor) (eV)	1.22(0.70)	0.5(0.60)	-	-
Standard deviation of Gaussian for donor (acceptor) (eV)	0.23(0.23)	0.21(0.21)	-	-
Capture cross section σ_c (σ) for donor-like Gaussian states (cm^2)	1.0 x 10^{-14} (1.0 x 10^{-15})	3.0 x 10^{-14} (3.0 x 10^{-15})	-	-
Capture cross section σ_c (σ) for acceptor-like Gaussian states (cm^2)	1.0 x 10^{-15} (1.0 x 10^{-14})	3.0 x 10^{-15} (3.0 x 10^{-14})	-	-
Total DOS D_n (cm^{-2})	-	-	1.0 x 10^9 1.0 x 10^{11}	-
Midgap density of state (cm^{-3} eV^{-1})	-	-	-	1.0 x 10^{10}
Characteristic Energy (eV)	-	-	-	0.56
Capture cross section for donor-like (cm^2)	-	-	1.0 x 10^{-14} (1.0 x 10^{-14})	1.0 x 10^{-14} (1.0 x 10^{-14})
Capture cross section for acceptor-like (cm^2)	-	-	1.0 x 10^{-14} (1.0 x 10^{-14})	1.0 x 10^{-14} (1.0 x 10^{-14})

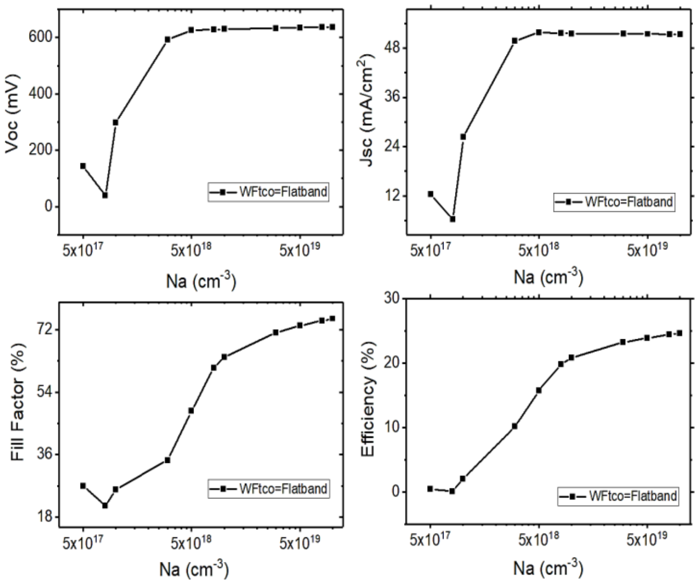

Figure 2. Doping N_A optimization results with flat band state on front contact

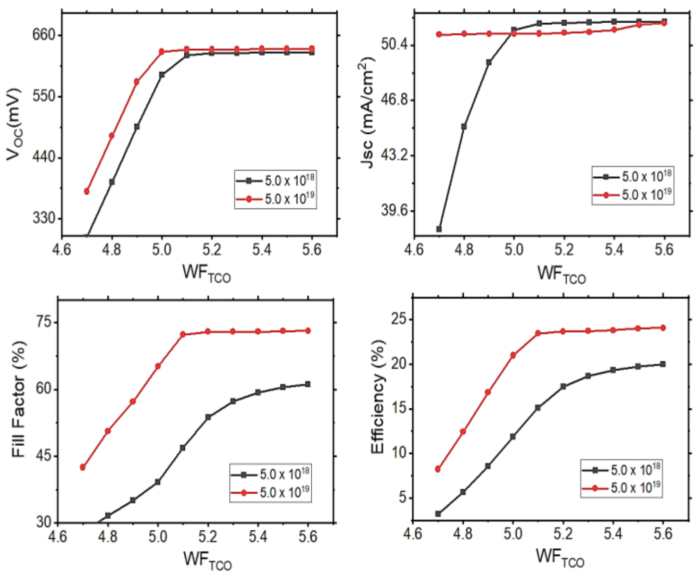

Figure 3. WFTCO variation on different N_A dopant concentration

Furthermore, adjustment on electrical field value from space charge region TCO/(p$^+$)a-Si:H would be equal to the ones from hetero layer (i)a-Si:H/(n)c-Si, this alignment of electrical field leads to strengthen the detach force between both electron-hole. Disparity between both moderate and high doping is defined on energy level spectrum in Figure 5. The graph implying that lowering WF_{TCO} value would made a Schottky barrier to rise. Forming a Schottky barrier could affect built-in potential voltage V_{bi} and efficiency percentage to decrease gradually. Referring to Figure 4, lower voltage solar cell output caused by Schottky barrier has made space charge region TCO/(p$^+$)a-Si:H electrical field controvert to hetero interface (i)a-Si:H/(n)c-Si causing generous amount of hole restrained for moving to front contact.

Appearance of Schottky barrier also takes place when the value of WF_{TCO} of front contact happen to be less than (p$^+$)a-Si:H layer work function, as stated on equation (13) [16].

$$\varphi_B = \left(\chi_{a-Si:H} - E_{G(a-Si:H)}\right) - WF_{TCO} \qquad (13)$$

where φ_B is barrier height, $\chi_{a-Si:H}$ as electron affinity on semiconductor layer, $E_{G(a-Si:H)}$ is energy gap, and WF_{TCO} as work function of thin conductive-oxide.

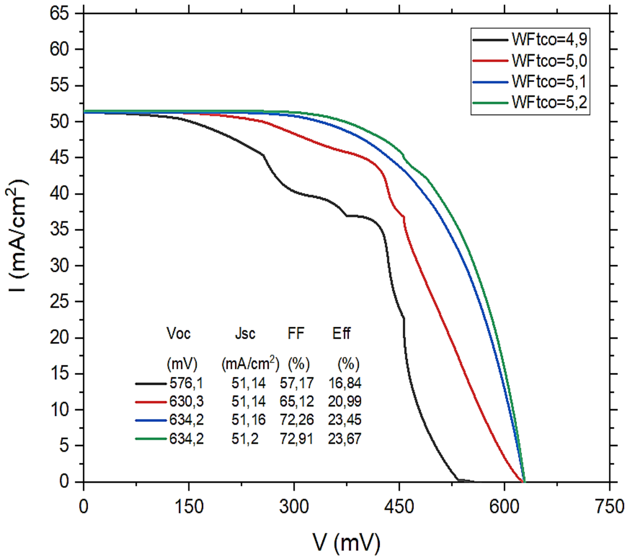

Figure 4. Solar cell I-V Characteristics on various front-contact work function (WF_{TCO}= 4,9 – 5,2) using high doping

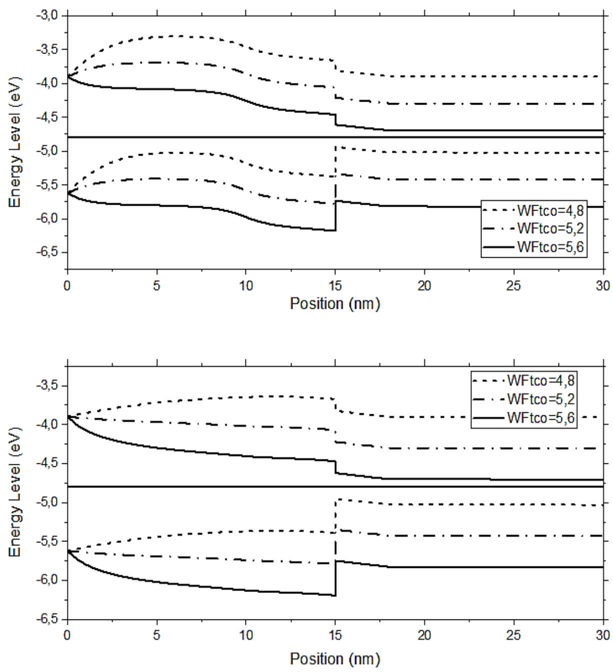

Figure 5. Energy band diagram with moderate (5.0 x 10^{18} cm^{-3}) and high-doped (5.0 x 10^{19} cm^{-3}) on different WF_{TCO} values.

Dangling-bond defect density (N_{tr}) represents fabrication defect condition on hetero layer for photovoltaic. Lower value of defect density means a semiconductor layer has been fabricated and well deposited, where the lower value would cause contrary results. Various experiments data of N_{tr} obtained by reference, varying from 1.0 x 10^{17} cm^{-3} to 1.0 x 10^{19} cm^{-3} [17]. The presented graph in Figure 6 shows a decline on all parameters, especially with fill factor and efficiency. Drastic drawdown on performances shown when N_A dopant approaching same value as N_{tr}. Lowering N_{tr} and fitting to N_A optimum value would be an optimum option to overcome the defect on material. This assumption matches with corresponding reference, where to maximize electrical results of photovoltaic, the amount of N_A dopant concentrate should be two times higher than defect density N_{tr} rate [15].

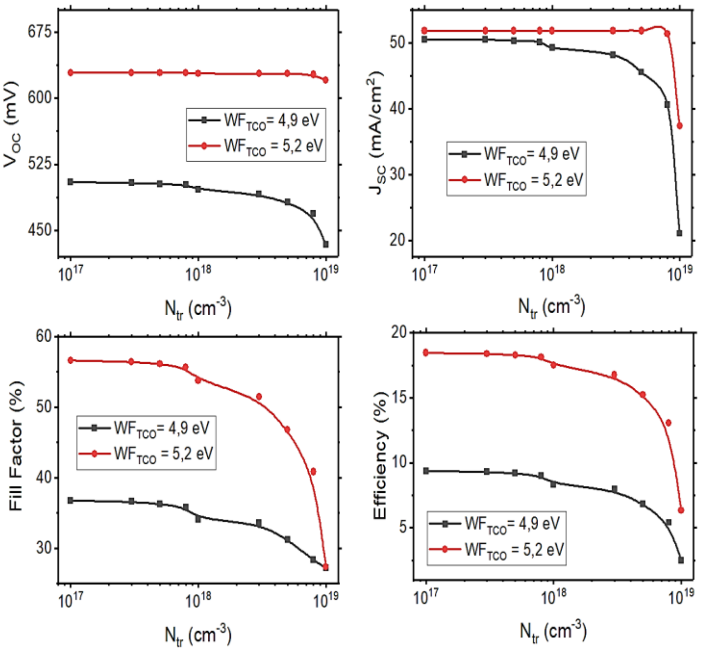

Figure 6. Defect density variation on (p$^+$) layer using moderate doping (N_A = 5.0 x 10^{18})

Maximizing defect density N_{tr} value for most advantageous system for both variation doping, N_{tr} value of 1.0 x 10^{18} cm^{-3} was used to observe other electrical properties. Figure 7 and Figure 8 display electrical field and recombination properties on different doping variation, by implementing 2 options of WF_{TCO} to examine the suitable optimization system. As observed in Figure 7(a), large electrical field produced using moderate doping N_A = 5.0 x 10^{18} cm^{-3} have a different value of total 4.69 x 10^7 V/cm. High electrical field would produce a large electron-hole to segregate which affect massive electrical generation. Significant change in electrical field is associated with a slow recombination rate as given in Figure 7(b). This also occurs by giving an intrinsic thin layer as prevention of decreasing electrical field on hetero layer, so the 'passivation effect' is able to boost~~ed~~ up.

According to Ghannam, et al (2016), applying high doping N_A = 5.0 x 10^{19} cm^{-3} is a better option than moderate doping [15]. In Figure 8, both WF_{TCO} variant does not show any notable contrast for electrical field and recombination rate, this circumstance is caused by high concentration doping covering the hetero defect on fabrication. Comparing the simulation results between moderate and high-doped, the research achieved an improved system to be applied for solar cell fabrication.

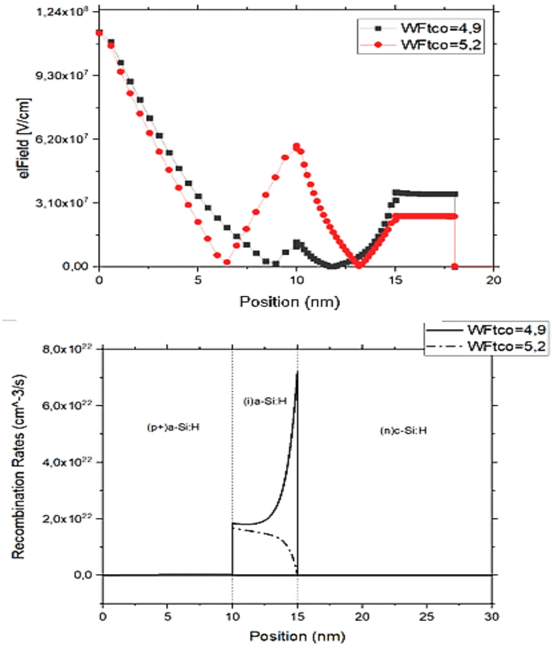

Figure 7. Electric field profile and recombination rates of solar cell with moderate doping (N_A = 5.0 x 10^{18} cm^{-3})

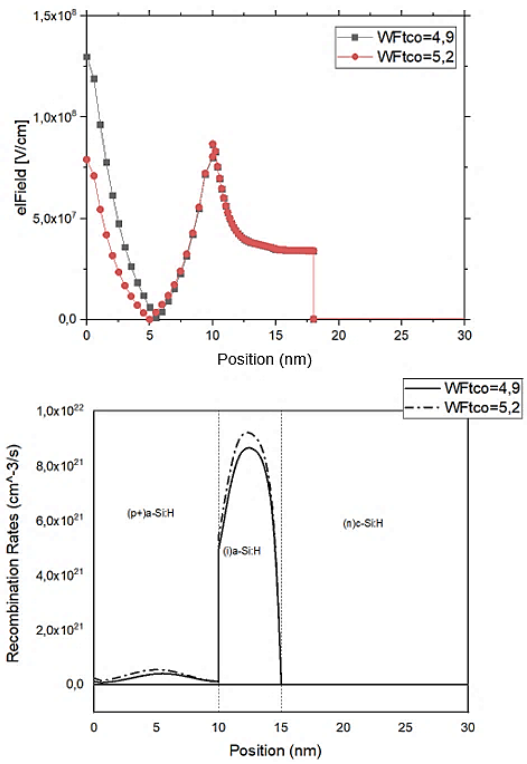

Figure 8. Electric field profile and recombination rates of solar cell with high doping (N_A = 5.0 x 10^{19})

The performance of the solar cell is significantly different between the two types of structure when a defect layer is added ~~at~~ to the hetero(i)a-Si:H/(n)c-Si:H interface. It can be seen in Figure 9 where the performance declines on data record with a structure that does not use a thin intrinsic layer (V_{OC} = 619.1 mV; J_{SC} = 32.36 mA/cm^2; FF = 65.7%; E_{ff} = 13.61%). The process of including a intrinsic thin layer at the hetero interface is an effort to provide a passivation effect and so lower the rate of recombination in solar cells. This is supported by the data showing that the addition of a defect layer at the interface (i)a-Si:H/(n)c- Si:H exhibited an improvement in performance with values (V_{OC} = 628.5 mV; J_{SC} = 51.84 mA/cm^2; FF = 53.63%; E_{ff} = 17.47%) showing a slight decline in the FF value but there was a significant increase in the short-circuit density J_{SC}, where the comparison of the two variations resulted in a difference of 19.48 mA/cm^2.

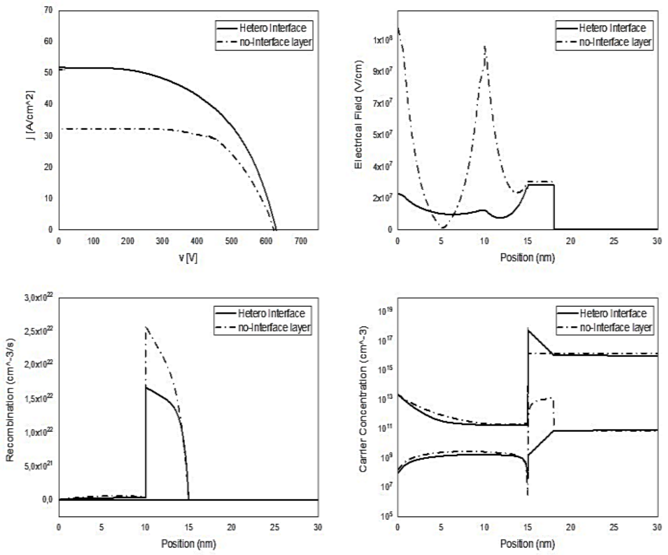

Figure 9. Internal profile comparison of thin film layer utilization on (i)a-Si:H/(n)c-Si with doping N_A = 5.0x10^{18} cm^{-3}, D_{it} = 1.0 x 10^{18} cm^{-3} dan WF_{TCO} = 5,2 eV.

Regarding the impact of a thin intrinsic layer on the hetero interface (i)a-Si:H/(n)c-Si:H, it results in field-effect passivity due to the presence of a strong electric field that allows the movement of tiny electrons on the hetero layer between a-Si:H/c-Si:H. Additionally, this passive effect results in a reduction of the layer's rate of recombination.

IV. CONCLUSION

When the WF_{TCO} value is low (<5.0 eV), a Schottky barrier forms at the front contact interface, hindering the movement of holes and reducing the number of holes reaching the front contact. However, when the front contact work function is much higher (>5.0 eV), an Ohmic-like contact is formed, which allows holes to be injected into the front layers and creates reverse barriers. Simulations of dangling-bond defect density reveal that a decline in solar cell performance occurs due to the inability of the doping concentration to compensate for the defect quantity in the material. To optimize photovoltaic modules, a balance must be struck between these two components, where the doping concentration must be greater than the defect density N_{tr} ($N_A \geq 2$ x N_{tr}). The simulation results show that the ITO/(p$^+$)a-Si:H/(i)a-Si:H/(n)c-Si/Al solar cell structure reaches a maximum efficiency of 23.67% (V_{OC} = 634.2 mV; J_{SC} = 51.2 mA/cm^2; FF = 72.91%, this result achieved on peak data as follows WF_{TCO} = 5,2 eV, Na (doping) = 5.0 x 10^{19} cm^{-3}, WF_{TCO} = 1.0 x 10^{18} cm^{-3}, D_{it} (interface defect) = 1.0 x 10^{10} cm^{-3}.

ACKNOWLEDGEMENT

This research is supported by Theoretical and Materials Physics Laboratory, Department of Physics, Mulawarman University.

REFERENCES

[1] T. Matsui *et al.*, "High-efficiency thin-film silicon solar cells realized by integrating stable a-Si:H absorbers into improved device design," *Japanese Journal of Applied Physics*, vol. 54, no. 8S1, p. 08KB10, Jul. 2015, doi: 10.7567/JJAP.54.08KB10.

[2] A. Sholih, D. Hamdani, S. T. Wicaksono, M. I. P. Hidayat, Y. Cahyono, and Darminto, "Numerical Simulation on Effects of TCO Work Function on Performance of a-Si:H Solar Cells," in *Functional Properties of Modern Materials II*, Oct. 2019, vol. 966, pp. 501–506. doi: 10.4028/www.scientific.net/MSF.966.501.

[3] M. Stuckelberger, R. Biron, N. Wyrsch, F.-J. Haug, and C. Ballif, "Review: Progress in solar cells from hydrogenated amorphous silicon," *Renewable and Sustainable Energy Reviews*, vol. 76, pp. 1497–1523, 2017, doi: https://doi.org/10.1016/j.rser.2016.11.190.

[4] W. H. Son, T. Y. Lee, S. Y. Choi, and D. Jung, "Effect of phosphorus doping on the performance of pin-type a-Si:H thin-film solar cells," *Molecular Crystals and Liquid Crystals*, vol. 662, no. 1, pp. 25–31, 2018, doi: 10.1080/15421406.2018.1466237.

[5] S. Prayogi, Y. Cahyono, I. Iqballudin, M. Stchakovsky, and D. Darminto, "The effect of adding an active layer to the structure of a-Si: H solar cells on the efficiency using RF-PECVD," *Journal of Materials Science: Materials in Electronics*, vol. 32, no. 6, pp. 7609–7618, Mar. 2021, doi: 10.1007/s10854-021-05477-6.

[6] K. Yoshikawa *et al.*, "Silicon heterojunction solar cell with interdigitated back contacts for a photoconversion efficiency over 26%," *Nature Energy*, vol. 2, no. 5, p. 17032, Mar. 2017, doi: 10.1038/nenergy.2017.32.

[7] C. Luderer, L. Tutsch, C. Messmer, M. Hermle, and M. Bivour, "Influence of TCO and a-Si:H Doping on SHJ Contact Resistivity," *IEEE Journal of Photovoltaics*, vol. 11, no. 2, pp. 329–336, 2021, doi: 10.1109/JPHOTOV.2021.3051206.

[8] D. Hamdani, Y. Cahyono, G. Yudoyono, and Darminto, "Band gap optimization of thin film a-si:H bifacial solar cells (bfscs) using afors-het," *Materials Science Forum*, vol. 966 MSF, no. i, pp. 409–414, 2019, doi: 10.4028/www.scientific.net/MSF.966.409.

[9] N. Hernández-Como and A. Morales-Acevedo, "Simulation of hetero-junction silicon solar cells with AMPS-1D," *Solar Energy Materials and Solar Cells*, vol. 94, no. 1, pp. 62–67, 2010, doi: https://doi.org/10.1016/j.solmat.2009.05.021.

[10] D. Hamdani, S. Prayogi, Y. Cahyono, G. Yudoyono, and D. Darminto, "The influences of the front work function and intrinsic bilayer (i1, i2) on p-i-n based amorphous silicon solar cell's performances: A numerical study," *Cogent Engineering*, vol. 9, no. 1, p. 2110726, 2022, doi: 10.1080/23311916.2022.2110726.

[11] D. Hamdani, Y. Cahyono, G. Yudoyono, and D. Darminto, "Performances analysis of heterojunction solar cells through integration of hydrogenated nanocrystalline silicon bilayer by using numerical study," *Molecular Crystals and Liquid Crystals*, vol. 725, no. 1, pp. 91–110, 2021, doi: 10.1080/15421406.2021.1922226.

[12] R. Stangl, C. Leendertz, and J. Haschke, "Numerical Simulation of Solar Cells and Solar Cell Characterization Methods: the Open-Source on Demand Program AFORS-HET," *Solar Energy*, Feb. 2010, doi: 10.5772/8073.

[13] D. Hamdani, S. Prayogi, Y. Cahyono, G. Yudoyono, and D. Darminto, "The Effects of Dopant Concentration on the Performances of the a-SiOx:H(p)/a-Si:H(i1)/a-Si:H(i2)/µc-Si:H(n) Heterojunction Solar Cell," *International Journal of Renewable Energy Development*, vol. 11, no. 1, pp. 173–181, Feb. 2022, doi: 10.14710/ijred.2022.40193.

[14] G. Ahmad, S. Mandal, A. K. Barua, T. K. Bhattacharya, and J. N. Roy, "Band Offset Reduction at Defect-Rich p/i Interface Through a Wide Bandgap a-SiO:H Buffer Layer," *IEEE Journal of Photovoltaics*, vol. 7, no. 2, pp. 414–420, 2017, doi: 10.1109/JPHOTOV.2016.2642644.

[15] M. Ghannam, Y. Abdulraheem, and G. Shehada, "Interpretation of the degradation of silicon HIT solar cells due to inadequate front contact TCO work function," *Solar Energy Materials and Solar Cells*, vol. 145, pp. 423–431, 2016, doi: https://doi.org/10.1016/j.solmat.2015.11.007.

[16] A. Belfar and H. Aït-Kaci, "Effect of incorporating p-type hydrogenated nanocrystalline silicon buffer layer on amorphous silicon n–i–p solar cell performances," *Thin Solid Films*, vol. 525, pp. 167–171, 2012, doi: https://doi.org/10.1016/j.tsf.2012.10.060.

[17] A. Ahmed, K. Riaz, H. Mehmood, T. Tauqeer, and Z. Ahmad, "Performance optimization of CH3NH3Pb(I1-xBrx)3 based perovskite solar cells by comparing different ETL materials through conduction band offset engineering," *Optical Materials*, vol. 105, p. 109897, 2020, doi: https://doi.org/10.1016/j.optmat.2020.109897.